PHYSICAL REVIEW A VOLUME 25, NUMBER 2 FEBRUARY 1982

Ultrarelativistic waves in overdense electron-positron plasmas

J. N. Leboeuf,* M. Ashour-Abdalla, T. Tajima,* C. F. Kennel,
F. V. Coroniti, and J. M. Dawson
Department of Physics, University of California, Los Angeles, California 90024
(Received 30 March 1981)

The interaction of singly periodic nonlinear waves of relativistic amplitude and electron-positron plasmas is investigated by means of fully self-consistent, relativistic, electromagnetic-particle computer simulation. When the frequency of a superluminous wave is slightly above the relativistic cutoff frequency, the initial waveform, be it sinusoidal or sawtooth (a self-consistent cold-fluid-theory solution), breaks up and creates a very hot plasma with a large particle flux $\Gamma \lesssim 2n_0c$ in the longitudinal direction. We find an important deviation from the cold-fluid-theory solution in the form of localized density spikes at the extrema of the wave magnetic field. For a wave frequency well above the cutoff, an initial sinusoidal waveform changes little but still creates a large longitudinal particle flow. Our observations of a large longitudinal flux of high-energy particles confirms a suggested mechanism for cosmic-ray acceleration.

I. INTRODUCTION

The electromagnetic waves emitted by the rotating magnetic dipoles of pulsars are believed to be so intense that the electron momentum in a single quivering oscillation far exceeds m_0c, where m_0 is the electron rest mass and c the speed of light.[1] When the waves are ultrarelativistic, and the ion quiver momentum is large, the difference between electron and ion rest mass becomes insignificant[2] and the plasma may be treated as an electron-positron medium. In addition, Sturrock[3] has suggested that pulsars may generate primarily an electron-positron plasma. Thus, for reasons of astrophysics as well as basic physics, it is of interest to study ultrarelativistic waves in an electron-positron plasma.

Nonlinear relativistic waves have been studied analytically using the cold-fluid plasma equations assuming a steady state.[2,4,5] These analyses have found a nonlinear sawtooth wave solution. The following simple argument leads one to expect a sawtooth wave in the steady state: For relativistic amplitudes, the current density is a square wave, which by integration of Ampere's law gives rise to a triangular or sawtooth-shaped magnetic field.[1] No experimental verification of such effects is yet feasible. To our knowledge, no time-dependent kinetic analysis of nonlinear relativistic waves has been carried out. Computer simulation has both of these capabilities. It can follow the exact orbits of many particles in self-consistent fields. Since computer simulation controls and diagnoses the experimental medium mathematically, without the physical limitations of experiments, it can study parameter regimes far removed from common experience. It will be used here to study the interaction of periodic electromagnetic waves with an overdense electron-positron plasma. As is known,[6] the relativistic electromagnetic wave can propagate in an overdense plasma because the wave fields oscillate the particles to relativistic energies, thereby reducing the effective plasma frequency (cutoff frequency). We use a fully self-consistent electromagnetic particle code with relativistic dynamics.[7,8] An electron-positron plasma with equal initial temperatures, cold or warm, is considered. The initial transverse electric and magnetic fields and particle momenta are chosen self-consistently. The input waveform may be either sinusoidal or sawtooth. The wave thereafter evolves self-consistently in space and time. These simulations will examine the effects of the plasma on the input waveform as it propagates, and the plasma's response to the wave fields. What waveform the input wave evolves to is of particular interest given the kinetic nature of the simulations and the theoretical prediction of a steady-state sawtooth solution from cold-fluid theory.[4]

The following physical picture emerges out of this investigation: (i) As is expected, the wave-particle interaction is stronger when the wave frequency is closer to the relativistic cutoff frequency; (ii) the wave evolved from an initial sinusoid is un-

steady and modulated by spiky density perturbations; (iii) a sawtooth input waveform with self-consistent particle perturbation, the nonlinear solution of the cold-fluid equations, is destroyed in roughly one wave period by similar spikes; (iv) intense particle acceleration in the direction of propagation takes place; (v) intense plasma heating is universally observed in a variety of initial conditions with most of the particles propagating forward; (vi) the system reaches a quasistationary state consisting of a heated forward propagating plasma containing a complex wave spectrum.

This paper is structured as follows. A succinct derivation of the sawtooth waveform is given in Sec. II, and its consequences for the energetics of the wave-plasma interaction are outlined. We describe the simulation model in Sec. III. Section IV is devoted to the study of sinusoidal input waveforms with frequencies both well above and close to cutoff. Section V deals with the propagation of a sawtooth input waveform in an electron-positron plasma. Section VI summarizes the energetics of the interaction in all three cases. The results of the simulations are summarized and their astrophysical implications discussed in Sec. VII.

II. THEORY

We present a short overview of the theory of ultrarelativistic waves in an electron-positron plasma, with emphasis on the consequences for the energetics of the interaction. As a model, we treat a linearly polarized wave where all quantities are functions of $\eta=\omega_w(t-x/\beta c)$, where $\beta=v_p/c$, the phase velocity $v_p=\omega_w/k$, with ω_w the wave frequency, k the wave number, and x the coordinate in the direction of propagation. Using Maxwell's equations, equations of motion for each particle species and equations of continuity, the equations describing particle momenta for each species may be cast into the form[1,2]

$$\frac{d^2p_\perp}{d\eta^2}+2(\omega_{p\alpha}^2/\omega_w^2)p_\perp/[\beta(1+p^2)^{1/2}-p_\parallel]=0\ , \tag{1a}$$

$$\beta p_\parallel-(1+p^2)^{1/2}=\gamma(\beta u_\parallel-1)=\text{const}\ , \tag{1b}$$

where p is the particle momentum in units of $m_\alpha c$, with rest mass m_α for each species α, $u=v/c=p(1+p^2)^{-1/2}$, and $\omega_{p\alpha}$ the nonrelativistic plasma frequency for each α species, and $\parallel$ and $\perp$ refer to directions with respect to the wave vector k. The relativistic factor γ is defined as $\gamma=(1+p^2)^{1/2}$. The two assumptions made to derive these equations are charge neutrality and that perpendicular currents generated by oppositely charged species are equal. Under the assumption $p>>1$ for most η, Eq. (1a) becomes independent of the rest mass, and an electron-positron plasma becomes a good approximation; henceforth we take $m_e=m_i=m_0$.

The equation for the electric field can be integrated to yield[2]

$$\frac{\partial\vec{E}}{\partial\eta}=(8\pi en_\alpha c/\omega_w)[\beta^2(\beta^2-1)^{-1}]\vec{u}_\perp\ , \tag{2a}$$

$$\approx(8\pi en_\alpha c/\omega_w)[\beta^2(\beta^2-1)^{-1}]^{1/2}\vec{e}_\perp\text{sgn}p_\perp\ , \tag{2b}$$

where

$$\vec{u}_\perp\approx\vec{e}_\perp(1-\beta^{-2})^{1/2}p_\perp\ .$$

The resulting sawtooth shape of the electric field shown in Fig. 1 is characteristic of superrelativistic waves. Also shown are the parallel and perpendicular particle momenta as a function of η. The sawtooth waveform implies that the Fourier coefficients of the even harmonics of the wave vector are zero, while those of the odd harmonics follow the decay law N_H^{-2}, where N_H is the odd-harmonic number. This implies that the energies of the odd-harmonic modes decay as N_H^{-4}.

Some scalings can be obtained from the above equations.[2] For instance, the maximum momentum achieved by the particles in the field of the wave is

$$p_{\max}=(\nu\pi/4)[\beta^2/(\beta^2-1)]^{1/2}\ , \tag{3}$$

where the wave strength parameter

$$\nu=(eE_w/m_0\omega_w c)>>1\ ,$$

with E_w the maximum field amplitude. Since $p>>1$, this relates the relativistic factor γ of the particles to ν and v_p. From Eq. (1b), $p_\parallel\approx\beta^{-1}p$ and the maximum parallel momentum is then

$$p_\parallel^{\max}=(\nu\pi/4)(\beta^2-1)^{-1/2}\ . \tag{4}$$

One also extracts from the theory that the particle flux $\Phi_p=m_0c^3\sum_\alpha\int_V dVp_\alpha$ and the electromag-

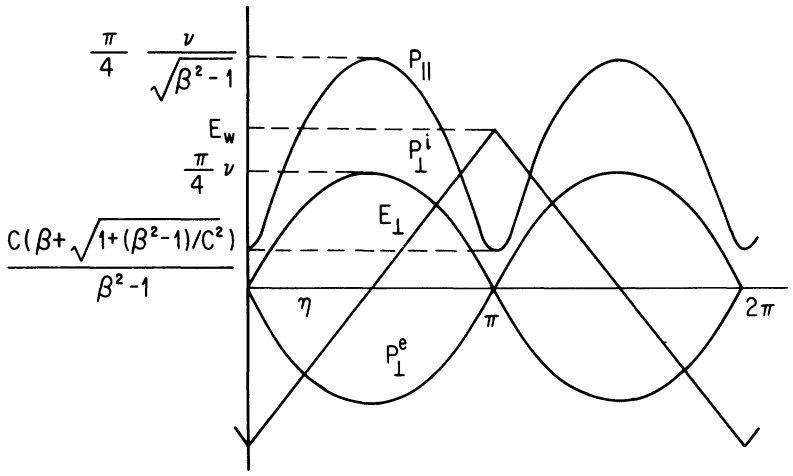

FIG. 1. Schematic illustration of the sawtooth waveform. The wave electric field, the parallel and perpendicular momenta for electrons and ions are drawn. The ordinate labels represent the excursion limits of the above quantities.

netic flux

$$\Phi_{\rm em}=(c/4\pi)\int_V(\vec{\rm E}\times\vec{\rm B})dV\ ,$$

integrated over the volume V are equipartitioned so that

$$\Phi_{\rm em}=\Phi_p=(c/12\pi\beta)E_w^2\ . \tag{5}$$

Finally, all charged particles are transported in the direction of wave propagation with the average velocity

$$v_{||}/c=c/v_p\ . \tag{6}$$

The natural upper bound on $v_{||}$ is in any case the speed of light c.

We can measure all the quantities listed above in our kinetic particle simulations. The simulation model in which this is done is described next.

III. SIMULATION MODEL

A one-and-two-halves-dimensional (one spatial and three velocity and field dimensions) version of our relativistic electromagnetic finite-size particle simulation code is used. The basic numerics may be found in Langdon *et al.*[7] or Lin *et al.*[8] Only one direction of spatial variation, the x direction, is allowed. The system size L_x is either 256Δ or 512Δ, where Δ is the cell size. Ten particles of each species per unit cell are loaded uniformly on the periodic spatial grid in the x direction. The particles of each species have equal mass and a charge of opposite sign so as to form an electron-positron plasma with equal temperatures. The particles have a Gaussian form factor with a characteristic radius of 1Δ to minimize noise. The wave amplitude E_w, its frequency ω_w, and the speed of light c are chosen so that the wave strength parameter

$$\nu=eE_w/m_0\omega_w c>>1\ ,$$

with the rest mass m_0, and e the positron charge; the particle quiver velocity $eE_w/m_0\omega_w$ normally exceeds the speed of light. The transverse fields and transverse particle momenta are specified self-consistently. The subsequent evolution of the system in space and time is followed over many wave periods.

Two aspects of the numerics deserve some comments. The time step Δt is limited essentially by the time for light to cross one grid length which is the largest propagation velocity of the electromagnetic wave and the largest particle velocity on the mesh (the Courant-Friedrich-Lewy condition). A more stringent limitation arises from the relativistic character of the waves. An upper bound in the time step is also set by the highest frequency $\omega_{\rm max}$ in the problem, so that $\omega_{\rm max}\Delta t\lesssim\frac{1}{2}$. Here, it is the relativistic cyclotron frequency $\omega=eB_w/m_0\gamma(i)c$, where B_w is the maximum magnetic field strength $[B_w=(kc/\omega_w)E_w]$ and $\gamma(i)$ is the relativistic factor of the ith particle associated with such fields. It is maximum for particles with zero or small momentum, i.e., $\gamma(i)\sim 1$, and the upper bound on the time step is then $\Delta t\lesssim m_0c/2eB_w$. A typical value of eB_w/m_0c is $100\omega_{pe}$, so that $\Delta t\lesssim 0.005\omega_{pe}^{-1}$, where ω_{pe} is the plasma frequency with the rest mass. This ensures the proper rotation by the Lorentz

force of all the particle momenta.

For the low-wave frequencies $\omega_w << \omega_{pe}$ we will concentrate on, this means an extremely small time step Δt and therefore a costly number of time steps for runs extending over a few wave periods. However, most of the particles have large relativistic factors when B is large, and they dominate the wave-particle interaction because of their large Lorentz force contribution. Only the few particles at or around zero momentum associated at the same time with large values of the magnetic field require such a small time step. Our tests in a few critical cases, such as the sawtooth wave propagation, indicate that there is no major difference in the physics even after a larger time step $\Delta t \sim 0.1\omega_{pe}^{-1}$ is used. Also, scaling down the wave amplitude to values of v where the operation of the code is well known and trusted[9] has reproduced the same qualitative features of wave propagation and plasma response observed in the present regime of very large v. One possible reason why choosing larger time steps does not lead to unphysical consequences may be that a particle which is not adequately described is most likely to move into the appropriate parameter regime at the next time step, since the acceleration is very large but the position error is at worst $2c\Delta t$. At worst, inaccurate treatment of particles with small momenta will introduce some noise in the system or a background fluctuation level, which is not altogether alien to nature. We have therefore chosen $\Delta t = 0.1\omega_{pe}^{-1}$ in most of the runs.

Strictly speaking, the particle size should also contract as the particle acquires large momenta. This is, unfortunately, costly to do because it involves the calculation of a different form factor for each particle at every time step. We have, therefore, introduced another approximation by keeping the size of the particle equal to one grid spacing in our model. This tends to overexaggerate the reduction of the plasma frequency mode by a factor $e^{-k^2a^2/2}$, where a is the fixed particle size and k the wave number. This form factor is in any case close to 1 (within 10%).[8] On the other hand, a more important physical reduction of the plasma frequency, a legitimate one, completely dominates, i.e., the relativistic momentum of the particle. Therefore, keeping the particle size fixed does not alter the physics to a great extent.

Our studies of the propagation of sinusoidal and sawtooth input waveforms in an electron-positron plasma, using the simulation model just described are presented in the next sections.

IV. SINUSOIDAL WAVES

Our first set of computer experiments investigated the evolution of a uniform input sinusoidal wave. We are primarily interested in overdense plasmas ($\omega_w < \omega_{pe}$), since this is where the most intense wave-particle interactions are expected.

A linearly polarized sinusoidal waveform propagating forward in the positive x direction is imposed at $t=0$ and the corresponding transverse fields are written as

$$E_y(x) = E_w \sin kx \ , \tag{7a}$$

$$B_z(x) = (kc/\omega_w) E_y(x) \ , \tag{7b}$$

$$E_z(x) = B_y(x) = 0 \ . \tag{7c}$$

The dimensionless field quantities are expressed in units of $(m\omega_{pe}^2\Delta/e)$, so that $E_w = vc\omega_w$, and $B_w = (kc/\omega_w)E_w$. The electrons' and positrons' momenta are perturbed for each ith particle with charge e_i according to

$$p_x(i) = p_z(i) = p_t \ , \tag{8a}$$

$$p_y(i) = \mathrm{sgn}(e_i/e) vc \cos[kx(i)] + p_t \ , \tag{8b}$$

with $k = 2\pi N/L_x$, where N is the mode number of the perturbation. The momenta are expressed in units of $m_0\omega_{pe}\Delta$. Initially, p_y and B_z are 90° out of phase. The quantity p_t is obtained from a Maxwellian distribution of momenta. We have found that whether it is present or not makes little difference to the results.

The frequency of the electromagnetic waves is modified from its nonrelativistic definition of $(\omega_p^2 + k^2c^2)^{1/2}$, where $\omega_p^2 = \omega_{pe}^2 + \omega_{pi}^2 = 2\omega_{pe}^2$ (for electrons and positrons) by relativistic mass effects. These commonly lead to the definition of the relativistic wave frequency as

$$(\omega_p^2/\gamma_{\max} + k^2c^2)^{1/2} \ ,$$

where $\gamma_{\max}$ is the maximum relativistic factor the particles achieve in the field of the wave, and $\gamma_{\max} = v$ initially.[6] This would yield a cutoff frequency for the electromagnetic wave of $\omega_{co} = \sqrt{2}\omega_{pe}/v^{1/2}$. However, the plasma particles span a range of γ's from $\gamma = 1$ to $\gamma = v$ in the field of the wave, and since the wave interacts with the whole plasma, we have settled upon a physically more appealing definition which involves the average of the relativistic factor over all of the plasma particles, $\langle\gamma\rangle$, so that

$$\omega_w = (\omega_p^2/\langle\gamma\rangle + k^2c^2)^{1/2} \ , \tag{9}$$

and an electromagnetic wave cutoff frequency of

$$\omega_{co}=\sqrt{2}\omega_{pe}/\langle\gamma\rangle^{1/2}\gtrsim\sqrt{2}\omega_{pe}/\nu^{1/2}\ . \tag{10}$$

This fine tuning of the wave frequency does not, however, lead to any significant differences in the results [as long as the wave frequency is truly above the global cutoff given by Eq. (10)]. Here we choose $\nu=100$ and $c=4\omega_{pe}\Delta$ (or $c=4v_{Te}$, if the initial thermal electron velocity $v_{Te}=\omega_{pe}\Delta$). The average relativistic factor is $\langle\gamma\rangle=63.6$ and the cutoff frequency is then, according to Eq. (10), $\omega_{co}=0.177\omega_{pe}$. The wave frequency is determined from Eq. (9) once the system size L_x is known and the mode number N of the perturbation (fixing the wavelength of the input wave) has been chosen.

A. Wave frequency well above cutoff

Our first run has $N=4$ for $L_x=256\Delta$, so that

$$kc=0.39>\omega_{pe}/\langle\gamma\rangle^{1/2}>\omega_{co}=0.177\omega_{pe}$$

or $\omega_w=0.43\omega_{pe}$. The wave frequency is well above the relativistic cutoff frequency, although the plasma is overdense. The wave period τ_w is $14.6\omega_{pe}^{-1}$ and the run extends over 14 wave periods, i.e., up to $\omega_{pe}t=200$.

Figure 2 illustrates the state of the wave-plasma system at $\omega_{pe}t=40$. We have plotted in Fig. 2(a) the momentum in the direction of propagation normalized to m_0c for each electron (represented by a dot) as a function of the distance x in units of the cell size Δ, or the p_x-x phase space; and in Fig. 2(b) the p_y-x phase space of these same electrons. Figure 2(c) is a plot of the z component of the wave magnetic field B_z, normalized to its maximum initial amplitude B_w as a function of distance x.

Figure 2(c) indicates that the wave shape at $\omega_{pe}t=40$ is almost identical to the input sinusoidal waveform. In fact, there was no departure at earlier or later times from the original sinusoid. This is understood as follows. Plasma effects come into the Ampere-Maxwell equation through the plasma current J_t:

$$-i\omega\vec{E}_t+4\pi\vec{J}_t=ci\vec{k}\times\vec{B}_t\ , \tag{11}$$

where the subscript t denotes the transverse component of the respective quantities, expressed here as Fourier-Laplace transforms in space and time. The maximum current density is of the order of $|J_t|=2n_0c$, where n_0 is the average number of particles per cell: The particles are readily accelerated to $\pm c$ by the large amplitude electromagnetic wave. When ω_w is large enough that $\omega_w|E_t|>4\pi|J_t|$, the character of Eq. (11) is predominantly that of the vacuum, i.e., $-i\vec{E}_t\approx ci\vec{k}\times\vec{B}_t$, and the plasma current effects are a secondary modification to the electromagnetic wave equation. For a nonrelativistic wave which propagates only in an underdense plasma, the larger the frequency of the wave the closer to the vacuum photon the character of the electromagnetic wave in the plasma is. For a relativistic wave, which can propagate not only in an underdense plasma but also in an overdense plasma, a similar

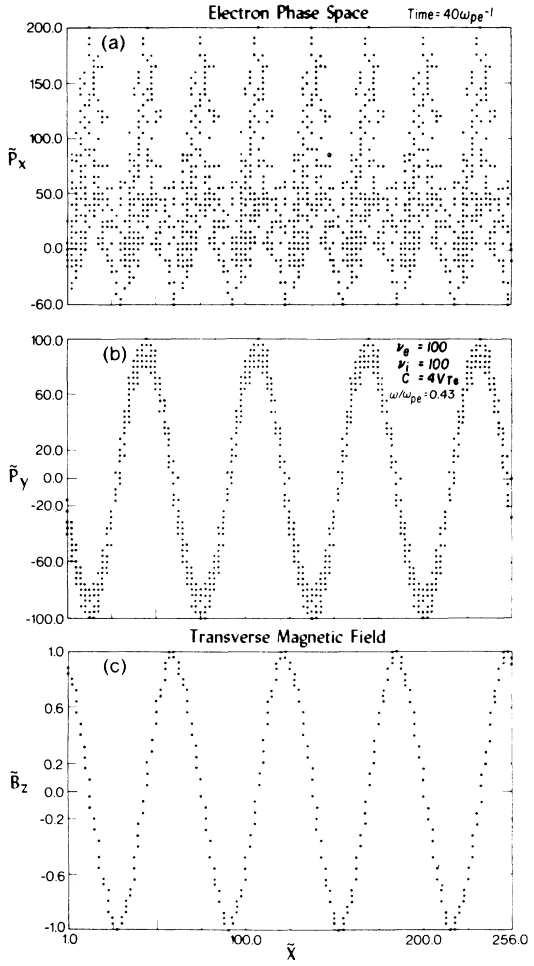

FIG. 2. Sinusoidal wave with frequency well above cutoff: (a) the p_x-x phase space of electrons at time $\omega_{pe}t=40$; (b) the p_y-x phase space of electrons at $\omega_{pe}t=40$. The momenta are normalized to m_0c; the distance to the cell size Δ. (c) Wave magnetic field B_z normalized to its initial maximum B_w as a function of the distance x at $\omega_{pe}t=40$.

tendency holds: The character of the wave is still close to a vacuum photon as long as ω_w is sufficiently above ω_{co} because of the relativistic mass effects.

The phase-space plots of the electron momentum p_x in Fig. 2(a) show substantial longitudinal acceleration up to $\gamma \sim 200$ in the direction of wave propagation. The positrons' behavior and acceleration is identical to that of the electrons. Twice as many forward streaks appear, at the positions of the maxima and minima of the magnetic field B_z. They are initially associated with the $\vec{v}_y \times \vec{B}_z$ force, which maximizes there because the transverse particle velocity v_y changes from $+c$ to $-c$ when B_z goes through a maximum or a minimum, and p_y and B_z are 90° out of phase. Heating in the x direction is also quite prominent; particles fill the large phase space (p_x-x) originally encircled by the cold energetic streak particles. Figure 2(b) indicates that the momentum in the y direction approximately preserves its original sinusoidal shape and magnitude. This tendency holds for the remainder of the run (up to $\omega_{pe}t = 200$). At $\omega_{pe}t = 120$ for instance, the particles have been accelerated forward in the x direction up to $p_x/m_0c \sim 300$ but the input waveform propagates essentially unchanged.

An examination of the energy of each magnetic normal mode as a function of time indicates that the input wave number, mode $N = 4$, has energies at least 4 orders of magnitude above all other modes, including its harmonics at all times. This confirms that the wave-number spectrum remains monochromatic and the wave shape sinusoidal throughout. We will now show that this is not the case when the frequency of the input sinusoidal waveform is close to the relativistic cutoff.

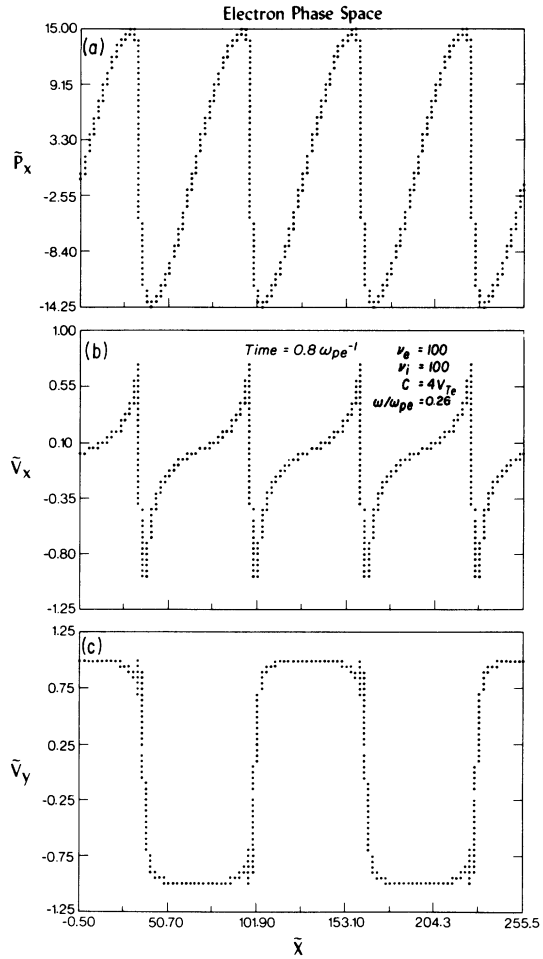

FIG. 3. Sinusoidal wave with frequency close to cutoff. Early time development ($\omega_{pe}t = 0.8$) of (a) the $p_x - x$ phase space of electrons, (b) their $v_x - x$ phase space, and (c) their $v_y - x$ phase space. The velocities are normalized to the speed of light c.

B. Wave frequency close to cutoff

When the wave frequency is close to the relativistic cutoff frequency, the wave characteristics deviate considerably from those in vacuum or in a tenuous plasma. Such a simulation is now presented. The cutoff frequency is still $\omega_{co} = 0.177\omega_{pe}$ for $v = 100$ and $c = 4\omega_{pe}\Delta$, so that $\langle\gamma\rangle = 63.6$ as before. Two wavelengths (i.e., mode number $N = 2$ is excited) fit into the system of size $L_x = 256\Delta$, so that $\omega_w = 0.265\omega_{pe}$, and $kc \sim \omega_p/\langle\gamma\rangle^{1/2}$. This means that $\omega_w |E_t| \lesssim 4\pi |J_t|$ in Eq. (11), and plasma effects dominate.

Multiple aspects of the data returned from this numerical experiment are presented in Figs. 3 through 7. Figures 3 and 4 show the state of the system very early ($t < 2\pi/\omega_{pe}$). Since p_y and B_z are of relativistic amplitude and 90° out of phase, v_y will change from $+c$ to $-c$, where p_y changes sign and B_z is maximum or minimum, to form the square-wave pattern of Fig. 3(c). Where v_y changes from $+c$ to $-c$, the longitudinal acceleration ($e\vec{v}_y \times \vec{B}_z/mc$) changes its sign from almost $+eB_w/m$ to $-eB_w/m$. Since v_y is proportional to eE_y initially, the direction and magnitude of the acceleration are charge independent. This acceleration gives rise to the large localized longitudinal momenta (p_x) of Fig. 3(a). Hence, whereas the initial longitudinal velocity v_x was initially zero, it quickly acquires values very close to $+c$ or $-c$, as shown in Fig. 3(b), where v_y changes sign at the extrema of B_z. Therefore, the density is

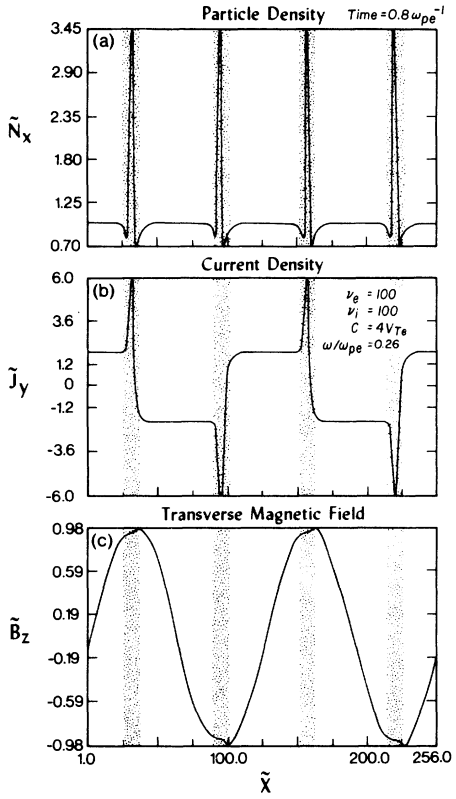

FIG. 4. Sinusoidal wave with frequency close to cutoff. Early time development ($\omega_{pe}t = 0.8$) as a function of the distance x of (a) the electron density normalized to the average density n_0, (b) the perpendicular plasma current density J_y normalized to n_0ec, and (c) the wave magnetic field B_z.

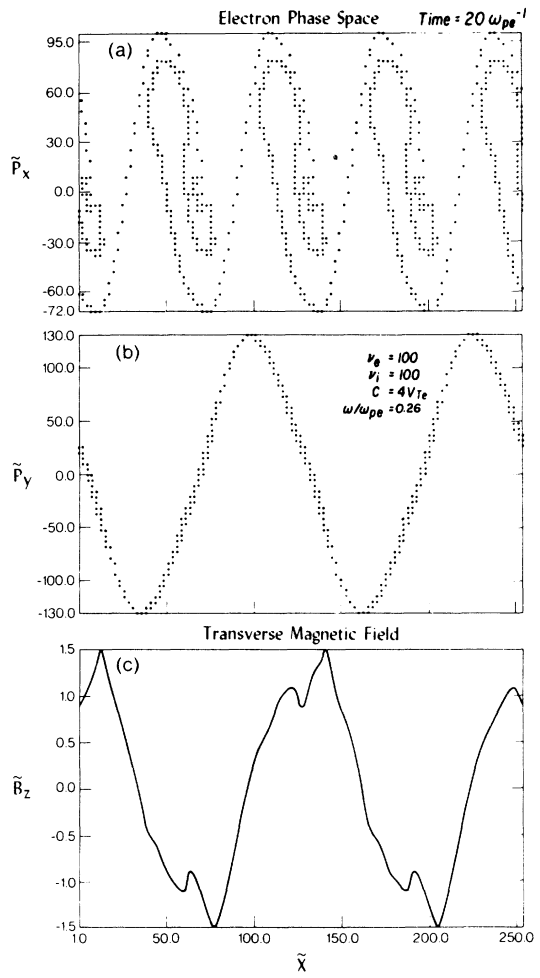

FIG. 5. Sinusoidal wave with frequency close to cutoff: (a) the $p_x - x$ phase space of electrons at time $\omega_{pe}t = 20$; (b) the $p_y - x$ phase space of electrons at $\omega_{pe}t = 20$; (c) wave magnetic field B_z as a function of the distance x at $\omega_{pe}t = 20$.

compressed there and in fact, from Fig. 4(a), it increases to three times the average density.

This delta-function density profile feeds back to the current density and almost completely obliterates its original square wave character as shown in Fig. 4(b), which if maintained would have resulted in sawtooth magnetic and electric fields. The spiky character of the current density in turn modifies the transverse fields, as shown in Fig. 4(c), and eventually leads to the breakup of the input waveform.

The long-time developement of the system presented in Figs. 5, 6, and 7 bears this out. From Fig. 5, even at $t = 20\omega_{pe}^{-1}$, strong distortion of the input sinusoidal waveform and phase space has set in on a time scale shorter than one wave period ($\tau_w \sim 24\omega_{pe}^{-1}$). At this time, there is as much forward as backward acceleration ($\gamma \sim 100$) in p_x. The phase difference between p_y and B_z is no longer 90°. Some departure in p_y from the initial sinusoidal perturbation is observed. From Fig. 6(c), the initially sinusoidal transverse electric field (E_y) has also acquired spiky perturbations. As displayed in Fig. 6(a), the initially uniform particle density exhibits substantial localized compression. Likewise, the current density in the y direction [Fig. 6(b)] is no longer akin to the initial square wave but is now dominated by a spiky structure correlated with the density spikes. The snapshots at $t = 180\omega_{pe}^{-1}$ of Fig. 7 show that the wave mainly accelerates particles forward in p_x up to $\gamma \sim 200$. By this time, intense heating in p_x has taken place, so that the thermal velocity is of the order of the speed of light. This is accompanied by slight heating in p_y and a significant departure from the ori-

ginal sinusoidal shape of the wave. The transverse magnetic field B_z is modulated by spikes. This also holds for the electric field. The particle density at this late stage ($t=180\omega_{pe}^{-1}$) shows a decay of the density spikes and a chaotic structure of less pronounced peaks.

Moreover, whereas originally the spikes in density occurred at the maxima and minima of the transverse fields (Fig. 4), they do not propagate at the group velocity of the wave c/β, where $\beta=v_p/c=1.3$ in the present run: They lag the electromagnetic wave; this dephasing produces in time the choppiness of the transverse fields. The velocity of the compressional wave is about $0.70c$, while the group velocity of the electromagnetic wave is $v_g\simeq 0.77c$. A similar phenomenon is observed for a sawtooth start and its significance will be discussed there in detail. Overall, the evolved waveform in the late stages has steepened compared to its initial sinusoidal one. It seems fairly steady but does not exhibit a tendency toward a sawtooth formation, as we shall now confirm.

The character of the wave, whether it is sawtooth or otherwise, can be established by scrutiny of the time-averaged wave-number spectrum, i.e., the magnetic energies of the normal modes averaged over the length of the run, which are plotted as a function of wave number in Fig. 8. This diagnostic shows that the input wave number (mode number $N=2$ or odd harmonic number $N_H=1$) is not the only prominent one, as it would have been if the sinusoidal shape had been preserved. However, only the odd harmonics of

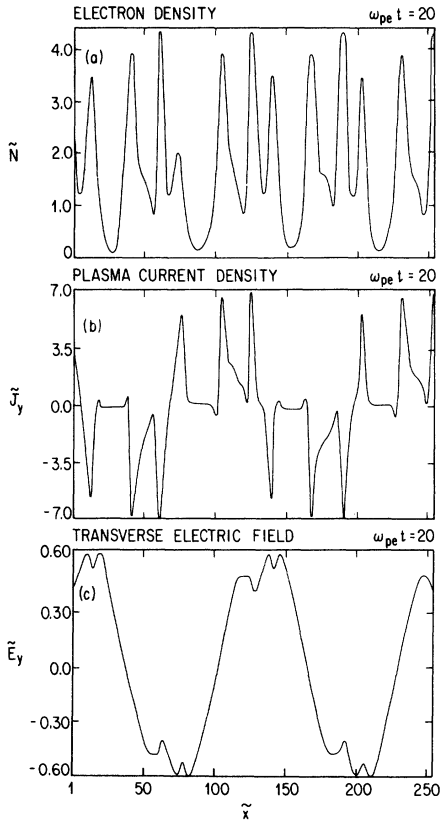

FIG. 6. Sinusoidal wave with frequency close to cutoff: (a) electron density versus distance x at $\omega_{pe}t=20$; (b) perpendicular plasma current density J_y versus distance x at $\omega_{pe}t=20$; (c) wave electric field E_y normalized to its initial maximum E_w as a function of distance x at $\omega_{pe}t=20$.

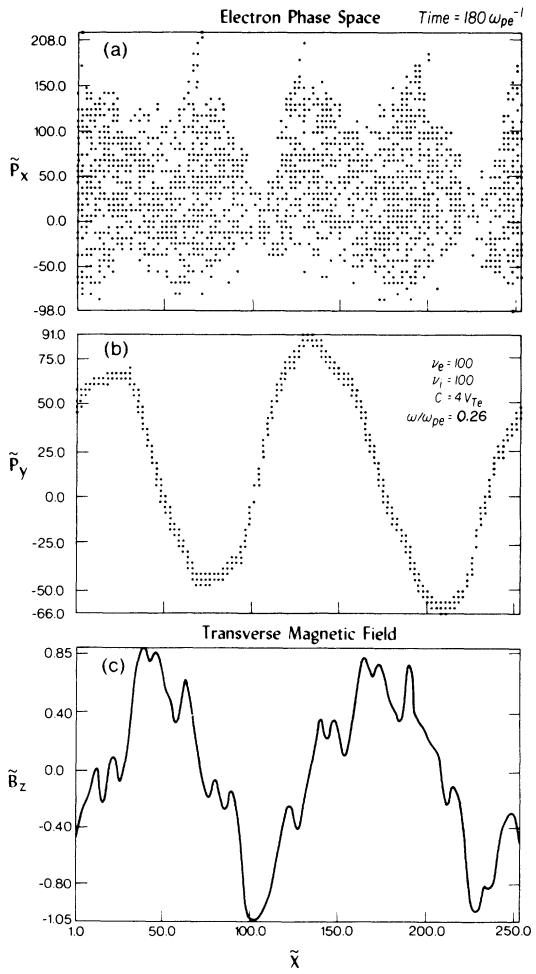

FIG. 7. Sinusoidal wave with frequency close to cutoff: (a) the p_x-x phase space of electrons; (b) the p_y-x phase space of electrons; (c) wave magnetic field B_z as a function of distance x. All are plotted at $\omega_{pe}t=180$.

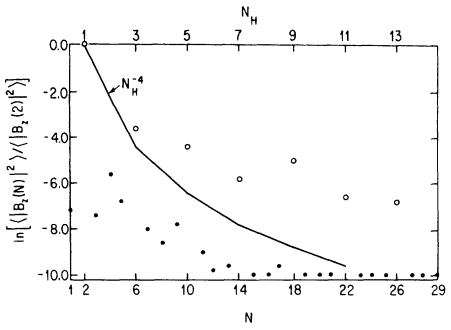

FIG. 8. Sinusoidal wave with frequency close to cutoff. Time-averaged magnetic wave-number spectra or energies per mode as a function of wave-number N and harmonic number N_H. The open circles indicate the energies of the odd harmonics, the dots the energies of the other modes. The solid curve follows the sawtooth decay law N_H^{-4}.

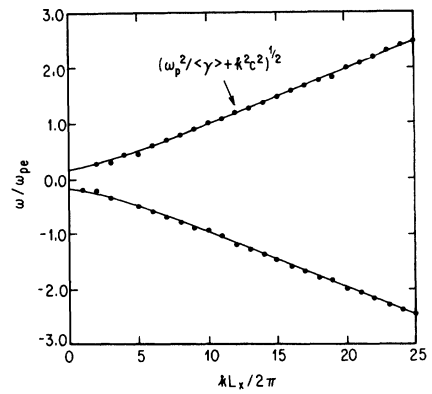

FIG. 9. Sinusoidal wave with frequency close to cutoff. Simulation dispersion relation, frequency ω versus mode number $N=kL_x/2\pi$. The dots label the simulation frequencies, the solid curves follow the theoretical prediction $\omega^2=\omega_p^2/\langle\gamma\rangle+k^2c^2$.

the fundamental wave number contain significant energy. Although this might indicate a tendency towards establishing a sawtooth (triangular) waveform, the sawtooth scaling law N_H^{-4} is not obeyed by spectral intensities of the odd harmonics. As is shown in Fig. 8, the ratio of these spectral intensities is much gentler than N_H^{-4}. This confirms the fact, apparent from Figs. 5, 6, and 7, that even though the wave has steepened (prominence of the odd harmonics), it has not evolved towards a sawtooth (the odd-harmonics spectral intensities do not decay as N_H^{-4}).

Temporal autocorrelations of the transverse electric fields and of the transverse magnetic fields over the length of the run have also been taken. The calculation of temporal autocorrelations involves a certain degree of time averaging. The simulation dispersion relation obtained from the frequency spectra of the various modes, the Fourier transforms of the temporal correlation function, is displayed in Fig. 9. The simulation dispersion relation is in good agreement with Eq. (9). This was also the case for the high-frequency sinusoidal input waveform. Here, even though the wave shape is distorted beyond recognition, the dispersion relation of the spiky waveform still conforms to the simple linear theory expression of Eq. (9), at least in a time-averaged sense.

We have also excited sinusoidal waves with frequencies purposely below cutoff ($\omega_w=\omega_{co}/2$ and $\omega_w=\omega_{co}/4$) to see how the plasma would react, since it is usually thought that electromagnetic waves with $\omega_w<\omega_p$ and relativistic ones with $\omega_w<\omega_{co}$ cannot propagate in the plasma (the wave vector becomes imaginary and the wave evanescent). Needless to say, the sinusoidal is destroyed in time and the evolved spiky waveform contains many wavelengths shorter than the input one. Heating in p_x occurs and only very few particles achieve large forward parallel momenta ($p_x/m_0c\sim 200$). However, the interesting observation is that the wave oscillates from propagating forward (its Poynting flux is positive), to backward or being reflected (its Poynting flux is negative), to forward again. Overall in time, the Poynting flux is positive and the wave propagates forward. Here, of course, the wave energy and momentum are already imbedded in the plasma at $\omega_{pe}t=0$. Also, since the plasma is much below cutoff ($\omega_w<<\omega_{co}$), it is so for both the forward propagating waves imbedded in it at $\omega_{pe}t=0$ and the backward waves generated by reflection; hence this oscillating direction of propagation. That it comes out to be forward overall is due to the preferential forward direction forced upon the plasma initially.

The results of the computer experiments on sinusoidal input waveforms can be summarized as follows: (i) Irrespective of the frequency of the initial wave, substantial acceleration of the particles in the direction of propagation is achieved through the $\vec{v}_y\times\vec{B}_z$ force. (ii) Substantial heating accompanies this acceleration. (iii) For wave frequencies close to cutoff, a delta-function density wave destroys the original sinusoidal wave field. (iv) Although the evolved waveform of B_z has steepened,

it is not sawtoothlike, a waveform one would expect if the square-wave current density profile is maintained.

The numerical experiments with a sawtooth input waveform described in Sec. V lead to similar conclusions.

V. SAWTOOTH WAVE PROPAGATION

We present a set of experiments where the input waveform is that given by the cold-fluid theory, i.e., a sawtooth waveform of B_z (or E_y) with self-consistent particle momenta.[4] The previous experiments showed that a sinusoidal waveform does not evolve into the cold-fluid steady state, the sawtooth solution, but into a relativistically hot plasma with twice as many peaks in density as in the fields, whose density peaks were caused by the $\vec{v}_y \times \vec{B}_z$ force. Although the initial sinusoid evolved into a seemingly quasistationary state, it may not have been an equilibrium start. This section will examine the evolution of a relativistic wave-cold plasma system, where the fields and particle momenta at time zero are theoretically in steady state. This equilibrium start is briefly presented and then the results of our numerical experiments under the equilibrium start are described. The sawtooth evolves to a final state similar to that of the sinusoid.

A. Sawtooth initialization

Since a spatially varying linearly polarized electromagnetic wave (E_y, B_z) of relativistic amplitude immediately accelerates both electrons and positrons to a speed very close to c in the transverse direction a square-wave velocity pattern results and, given a uniform density, so does a square-wave transverse current density $J_y \simeq \pm n_0 ec$. In the steady state, $B_t \simeq \pm 4\pi e n_0 x$ and the electromagnetic wave assumes a sawtooth (or triangular) wave shape as schematically illustrated in Fig. 1. The formal analysis of Kennel and Pellat[4] also yields the self-consistent initial perturbation of the momentum in the direction of propagation. Their solution of the cold-fluid equations yields the following relationship between fields and particle momenta:

$$p_x = c[V_{x0} + (\alpha\nu^2/2\beta)(1-a^2)] , \tag{12a}$$

$$p_y = \mathrm{sgn}(e_i/e)\frac{\alpha\nu^2 c}{2\gamma^*}[(1-a^2)(1-a^2+q)]^{1/2} , \quad -1 \le a \le 1 \tag{12b}$$

$$p_z = 0 . \tag{12c}$$

The parameters in the above are defined as

$$a = E_y/E_w, B_z = E_y/\beta , \tag{13a}$$

$$\beta^2 = \gamma^{*2}/(\gamma^{*2}-1),\ \gamma^{*2} = \beta^2/(\beta^2-1); \tag{13b}$$

$$\alpha = \tfrac{1}{2}\omega_w^2/\omega_{pe}^2 , \tag{13c}$$

$$q = 4\gamma^{*2}/\alpha\nu^2, V_{x0} = \gamma^*/\beta , \tag{13d}$$

where E_w is the peak wave amplitude. The dispersion relation is written as

$$\pi\gamma^{*4}/2 = \alpha\nu . \tag{14}$$

We have chosen $c = 4\omega_{pe}\Delta$, $\gamma^* = \sqrt{3/2}$, $\beta = \sqrt{3}$, and two wavelengths to fit into $L_x = 512\Delta$, so that $\lambda = 256\Delta$. This fixes $\omega_w = 0.17\omega_{pe}$, $\alpha = 1.44 \times 10^{-2}$, $q = 1.913 \times 10^{-2}$, $\nu = 133.06$, and consequently $E_w = 90.50$ and $B_w = 52.25$. Moreover, theory predicts that with these initial conditions the density should be uniform and the particles' velocities in the x direction equal to V_{x0} at $t = 0$. The initial sawtooth is shown in Fig. 10. It was verified that $v_x = V_{x0}$ at $t = 0$. Uniform spatial loading ensures uniform density. From the wave point of view at $t = 0$, there is no energy to speak of in the even harmonics of the principal mode number $N = 2$, and the energy content between odd harmonics follows the $1/N_H^4$ law characteristic of a triangular wave.

As is shown next, the sawtooth waveform does not survive.

B. Simulation results

As is clear from Figs. 11, 12, and 13, early distortion of the input waveform sets in for $t \sim \tau_w = 37\omega_{pe}^{-1}$. Spikes again appear in the transverse fields that almost completely obliterate the triangular pattern. Density plots reveal a compression region, again associated with maxima of B_z, where v_y changes from $+c$ to $-c$, just as in the sinusoidal start. At time $t = 120\omega_{pe}^{-1}$, the particles have acquired $\gamma \sim 200$ in the direction of propagation. Note also the longitudinal heating with a thermal spread of the order of the speed of light.

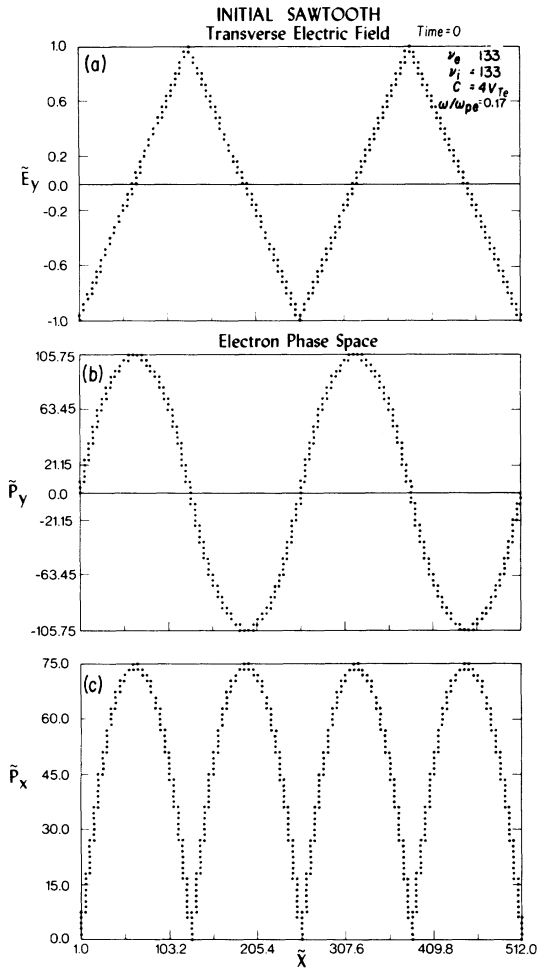

FIG. 10. Sawtooth wave. (a) initial profile of the wave electric field E_y as a function of distance x; (b) initial $p_y - x$ phase space of the electrons; (c) initial $p_x - x$ phase space of the electron.

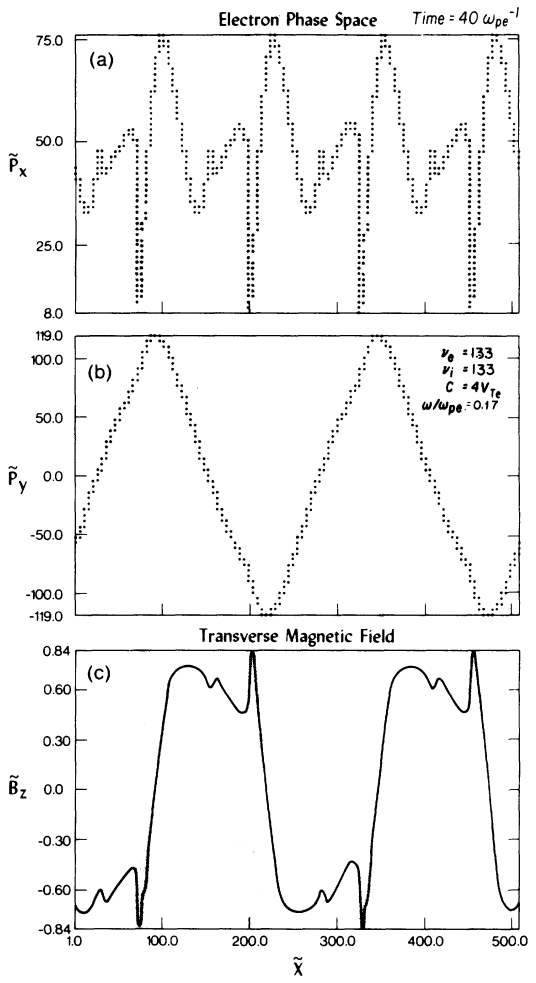

FIG. 11. Sawtooth wave. Snapshots of the system at $\omega_{pe}t = 40$: (a) electrons $p_x - x$ phase space; (b) electrons $p_y - x$ phase space; (c) wave magnetic field B_z versus distance x. The shaded regions correspond to the density maxima.

The initial development of the system was diagnosed and the same scenario as for the sinusoidal waveform holds: onset of a delta-function density wave which obliterates the square-wave current density; hence, disappearance of the input sawtooth waveform. The breakup of the sawtooth by the spikes did take longer, however, (of the order of one wave period $\tau_w \simeq 37\omega_{pe}^{-1}$). The group velocity of the sawtooth is slower than that of the low-frequency sinusoidal wave, i.e., $v_g = c/\sqrt{3}$ for the sawtooth compared to $c/1.3$ for the sine wave, so that the dephasing did not become apparent until a later time. This dephasing is emphasized in Fig. 13 where the shaded regions indicate the position of the spikes in density at $\omega_{pe}t = 120$. Once the spikes are formed, the wave never recovers its original sawtooth shape. The spiky waveform has been found to persist in runs covering 50 wave periods. This behavior has been verified to be independent of the system length, the mode number excited, the number of particles per wavelength, and whether the plasma is hot or cold at $\omega_{pe}t = 0$. Runs with impractical time steps satisfying $\Delta t < m_0 c/2eB_w$, as stipulated in Sec. III, also gave almost identical results to those with coarser time steps. This is also true of the sinusoidal input waveforms presented in Sec. IV.

The appearance of delta-function-like density compression at the extrema of B_z is intriguing and

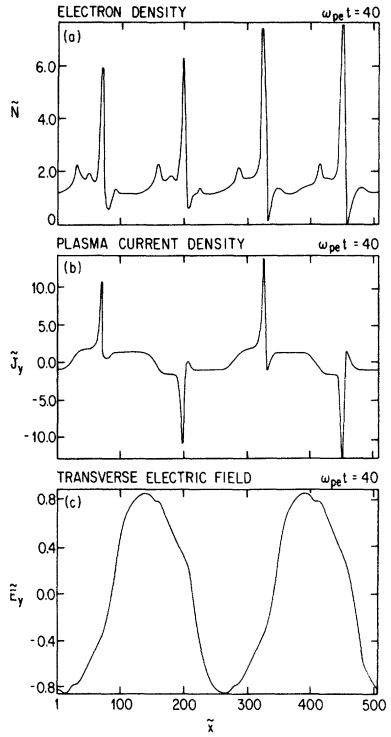

FIG. 12. Sawtooth wave. Snapshots of the system at $\omega_{pe}t = 40$: (a) electron density, (b) plasma current density J_y, (c) wave electric field E_y, all as a function of distance x.

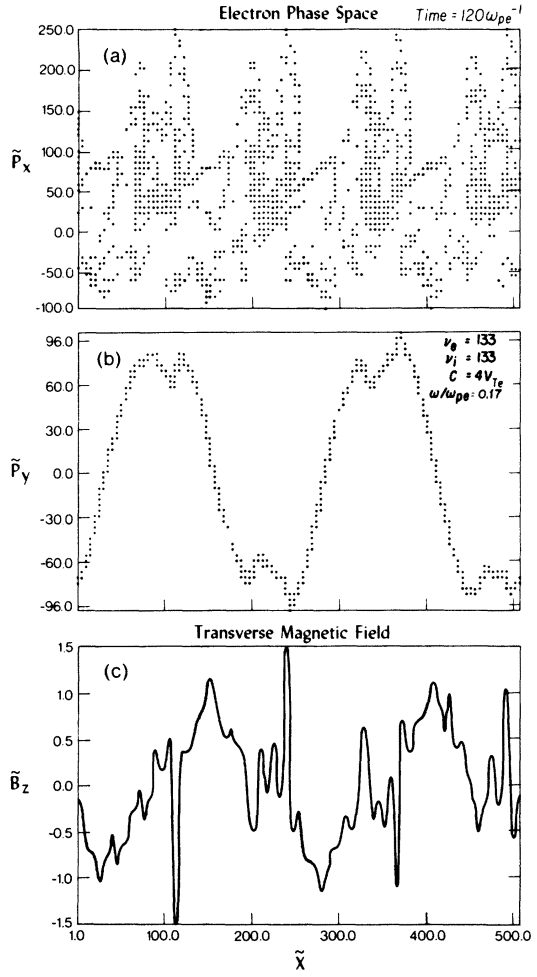

FIG. 13. Sawtooth wave. Snapshots of the system at $\omega_{pe}t = 120$: (a) electrons $p_x - x$ phase space; (b) electrons $p_y - x$ phase space; (c) wave magnetic field B_z as a function of distance x. The shaded regions correspond to the density spikes.

interesting. First, in the cold-fluid theory, the longitudinal momentum equation reads

$$\frac{dp_x}{dt} = \frac{\partial p_x}{\partial t} + v_x \frac{\partial}{\partial x} p_x = \frac{e}{c} \vec{v}_y \times \vec{B}_z \ . \tag{15}$$

The sawtooth solution, Eqs. (13) and (14), equates $v_x(\partial/\partial x)p_x$ to $(e/c)\vec{v}_y \times \vec{B}_z$ at $t = 0$. Therefore, p_x does not initially change in the laboratory frame. At the same time, the continuity equation at $t = 0$ reads

$$\frac{\partial}{\partial t} n + \frac{\partial}{\partial x} n v_x = \frac{\partial n}{\partial t} + n \frac{\partial}{\partial t} v_x = 0 \ , \tag{16}$$

where we used n is constant at $t = 0$. Since v_x is uniform in Eq. (16), n does not change either in the laboratory frame at $t = 0$. A perturbation in v_x, however, can destroy the sawtooth waveform in a scenario similar to the one presented in Sec. IV. It may be worth pointing out that the so-called space-independent frame for a superluminous wave[4,5] (sometimes called the frame where photon momentum is zero and only photon mass remains[9]) leads to invariance of density. This is only true, however, if the wave number of the density modulation is associated with that of the photon.[9] Therefore, once the perturbation contains a wave number different from $N = 2$, in our case, it is no longer space-independent (invariant), and there is no reason to believe that the density remains constant.

Time autocorrelations of the transverse electric and magnetic fields did yield a dispersion relation similar to Fig. 9, again indicating, that however distorted the waveform, its dispersion still follows the linear theory estimate of Eq. (9). We have plotted in Fig. 14 the time-averaged spectral inten-

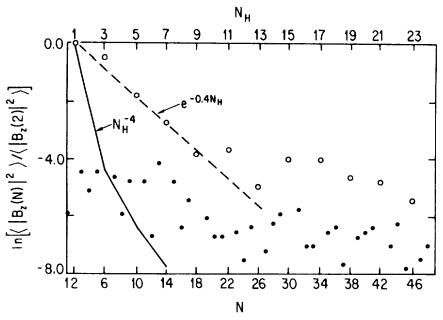

FIG. 14. Sawtooth wave. Time-averaged magnetic wave-number spectra or energies per mode as a function of mode number N and odd-harmonic number N_H. The open circles indicate the energies of the odd harmonics, the dots the energies of the other modes. The solid curve follows the sawtooth decay law N_H^{-4}. The simulation decay law $e^{-N_H/2.5}$ is plotted as a dashed line.

sities or mode energies as a function of mode number (N) and odd-harmonic number (N_H). At $\omega_{pe}t=0$, the wave-number spectra of the wave electric and magnetic fields obey the N_H^{-4} law between odd harmonics of the input mode $N=2$. It is also true that initially the even harmonics have negligible (i.e., thermal) energies. Figure 14 indicates that the even harmonics do not contain or gain a significant amount of energy throughout the run. Furthermore, the time-averaged energies of the odd harmonics are at least two orders of magnitude above the even. However, Fig. 14 shows that the odd harmonics do not follow the N_H^{-4} decay law that preservation of the sawtooth input waveform would have required. The decay is much gentler, as it was for the low-frequency sine wave, and here approximately scales as $e^{-0.4N_H}$ for the first few harmonics, except for $N_H=3$. The third harmonic achieves roughly the same energy as the fundamental mode $N=2$ or $N_H=1$. It is possible to speculate that the nonlinear interaction between the two defined modes observed at early times leads to a "stochastic" spectrum at late times, such as that found by Wersinger, *et al.*[10] We have not checked this suggestion in detail.

Even though the sawtooth wave shape is not preserved, particles are both accelerated in the direction of propagation to large momenta and substantially heated. We examine in Sec. VI the energy, momentum, and flux exchange between electromagnetic waves and particles for both sinusoidal and sawtooth starts.

VI. ENERGETICS OF THE RELATIVISTIC WAVE-PLASMA INTERACTION

The behavior of the maximum momentum in the direction of propagation, the partition of energy between fields and particles, the average velocity the plasma acquires in the field of the wave, and the partition of flux between waves and particles is compared with the theoretical estimates of Sec. II for both input sinusoidal waves and sawtooth waves. We also present an illustration of the energy distribution of the particles accelerated in the direction of propagation, of interest for the production of cosmic rays.

For the input sinusoidal wave well above cutoff of Sec. IV, both electrons and positrons gain equal and large net momenta from the waves. Energy and momentum exchange between the waves and the particles saturates at $\omega_{pe}t=100$ or after 7 wave periods. A steady state has been reached with the maximum momentum achieved by the particles in the x direction remaining nearly constant at $p_x/m_0c\simeq 300$, as compared to its value of zero at $\omega_{pe}t=0$. Note also that initially the maximum perpendicular momentum $p_y/m_0c=v=100$ here. The maximum parallel momentum achieved exceeds the theoretical estimate $p_x/m_0c\simeq 175$ from Eq. (4) of Sec. II. The total kinetic energy saturates at twice its initial value and thus represents $\frac{1}{3}$ of the wave energy (an equal amount, i.e., $\frac{1}{6}$, goes to electrons and positrons) as compared to $\frac{1}{6}$ initially.

A particle flux is generated only in the x direction, indicating a transfer of momentum from wave to particles only in the direction of propagation. We have plotted in Fig. 15(a) the average velocity $v_{||}$ in the direction of propagation for electrons (an identical value holds for positrons) as a function of time. The steady-state velocity is measured to be $v_{||}/c=0.52$. Equation (6) of Sec. II yields $v_{||}/c\simeq 0.9$, so that the simulation value is 60% of the theoretical estimate, which may therefore be an upper bound.

We have also measured the transfer of flux between fields and particles. In the simulation, the total flux is defined at each instant of time as

$$\Phi=c/4\pi\int_{L_x}(\vec{E}\times\vec{B})dx+c^2\sum_{\alpha}\int_{L_x}p_\alpha dx\ , \quad (17)$$

where the first term on the right-hand side is the electromagnetic flux Φ_{em}, the second the particle flux Φ_p, and the sum over α includes both electron and positron contributions. The integration is per-

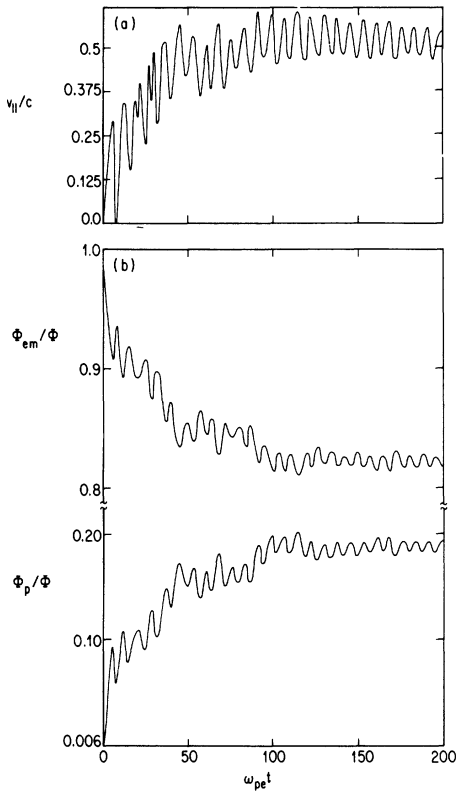

FIG. 15. Sinusoidal wave with frequency well above cutoff: (a) average parallel velocity $v_{||}/c$ as a function of time; (b) electromagnetic flux Φ_{em} and particle flux Φ_p normalized to the total flux Φ as a function of time.

formed over the system length L_x. The total flux Φ as defined in Eq. (17) is conserved in the simulation. We have plotted in Fig. 15(b) Φ_{em} and Φ_p normalized to the total flux Φ as a function of time. Equipartition of flux, as predicted by Eq. (5), is not achieved in the steady state: Φ_p nevertheless accounts for a substantial 25% of Φ_{em} as compared to a negligible 0.6% at early times. There is then substantial transfer of energy, momentum, and flux from waves to particles even though the wave remains sinusoidal throughout the interaction.

The energetics of an input sinusoidal waveform with frequency close to cutoff can be summarized as follows. Both electrons and positrons gain equal energy and momentum from the waves. An apparent steady state is quickly reached around $\omega_{pe}t=40$ or about two wave periods. The maximum parallel momentum achieved is $p_x/m_0c\sim 200$. Equation (4) on the other hand yields $p_x/m_0c\sim 90$. While the simulation value exceeds the theory by a factor of 2, there is a tendency for the maximum parallel momentum to decrease as the phase velocity increases {since $p_x/m_0c=(v\pi/4)[c^2/(v_p^2-c^2)]^{1/2}$ from Eq. (4)}, between the high-frequency sine wave run ($p_x/m_0c\sim 300$ and $v_p/c\simeq 1.095$) and the low-frequency sine wave run ($p_x/m_0c\sim 200$ and $v_p/c\simeq 1.35$). Likewise, the net increase in kinetic energy is only a factor 1.3 here as compared to a factor 2 for the high-frequency sine wave.

The parallel velocity of the electrons $v_{||}/c$ and the total particle flux Φ_p and electromagentic flux Φ_{em} are displayed as a function of time in Fig. 16 for the input sinusoidal waveform with frequency close to cutoff. The steady-state value of the average parallel velocity is $v_{||}/c\simeq 0.35$. The theoretical prediction is $v_{||}/c=0.75$ from Eq. (2); the simulation value is then about 50% of theory. Nevertheless, the tendency to decrease as the phase velocity increases also appears in the simulations. The reduction factor is, however, 1.5 times the ratio of the phase velocities between the high-frequency

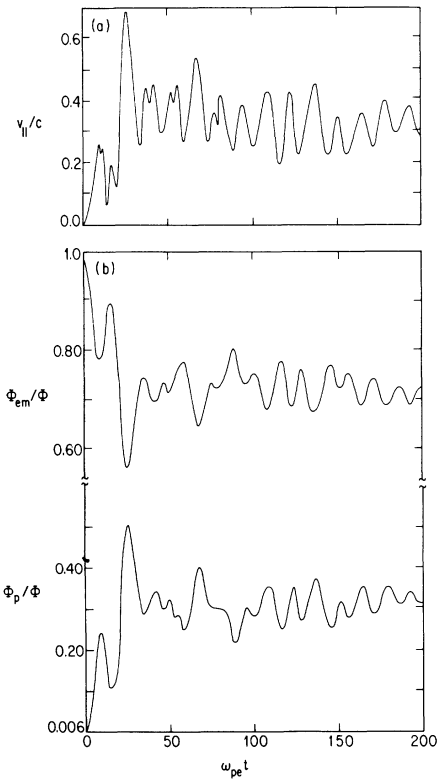

FIG. 16. Sinusoidal wave with frequency close to cutoff: (a) average parallel velocity $v_{||}/c$ as a function of time; (b) electromagnetic flux Φ_{em} and particle flux Φ_p normalized to the total flux Φ as a function of time.

sine wave run and the low-frequency sine wave one. Moreover, while equipartition of flux between particles and fields is not achieved in Fig. 16(b), Φ_p now accounts for about 50% of Φ_{em} in the steady state as compared to a negligible fraction initially and to 25% for the sinusoidal input waveform with frequency well above cutoff. More flux is then transferred from the fields to the particles as the frequency gets close to cutoff and the waveform has steepened from its original sinusoidal shape.

For the sawtooth input waveform of Sec. V, the energy and momentum exchange between the wave and the particles presents an oscillatory behavior, with field and kinetic energies settling down to their initial values in the apparent steady state. Note that initially the kinetic energy is 1.75 times larger than the wave energy. There is nevertheless a net forward acceleration of the particles, with a maximum parallel momentum around $p_x/m_0c = 200$, as compared to $p_x/m_0c = 75$ initially. The average parallel velocity is maintained at its initial value of 60% of the speed of light. Equipartition of flux is approximately satisfied initially and, while oscillatory, the fluxes preserve a rough equipartition in time. At $\omega_{pe}t = 0$, energy, momentum, parallel velocity and flux satisfy the theoretical prescriptions laid out in Sec. II. Even though the sawtooth waveform is not preserved, these prescriptions are approximately satisfied throughout the simulation, save for the oscillatory behavior of these quantities and the net gain in peak parallel momentum.

The sawtooth wave theory,[2,4] while it does not reproduce the exact behavior of field and particle quantities in the simulations, might still be used as a rough guideline to the energetics of the interaction between an ultrarelativistic electromagnetic wave and an electron-positron plasma. However, kinetic simulations yield results beyond the reach of the cold-fluid theories. We illustrate this by showing the energy distribution of the particles accelerated by the waves in the direction of propagation. This is done using the momentum distribution of the particles $f(p_x)$; since $p_x/m_0c >> 1$, $f(p_x)$ represents the distribution of relativistic factors or energies of the plasma particles. We have plotted three such distributions for electrons in the steady state at $\omega_{pe}t = 200$ in Fig. 17 for (a) the sinusoidal input waveform with frequency well above cutoff of Sec. IV, (b) the sinusoidal input waveform with frequency close to cutoff, and (c) the sawtooth input waveform of Sec. V. The energy distributions from all three experiments are qualitatively similar: A high-energy and high-density tail appears in the direction of propagation. Heating is also apparent from the broad width of the distribution around $p_x/m_0c = 0$. Relativistic waves with frequency well above cutoff yield more of the most highly energetic particles than the other two cases.

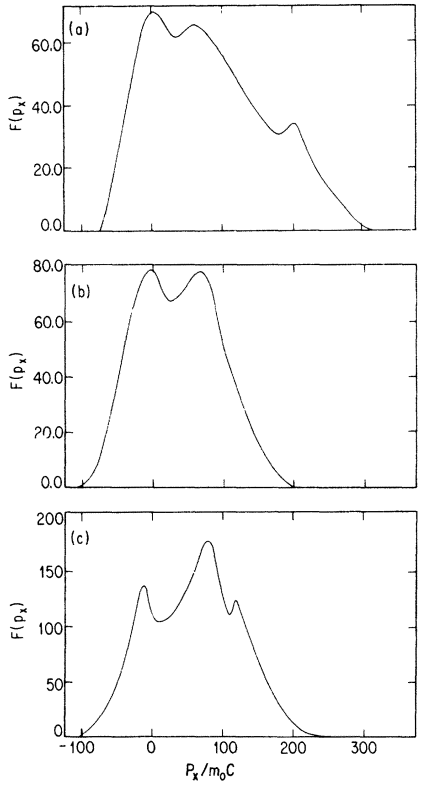

FIG. 17. An illustration of the energy distribution of the electrons in the steady state at $\omega_{pe}t = 200$. The parallel or p_x momentum distribution function $f(px)$ as a function of p_x for (a) the sinusoidal wave with frequency well above cutoff, (b) the sinusoidal wave with frequency close to cutoff, and (c) the sawtooth wave.

VII. DISCUSSION

A recent theory by Asseo *et al.*[11] proposed a Weibel-type instability[12] to explain the breakup of the sawtooth. Since $p_\perp >> p_{||}$ initially, the wave will grow at the expense of $p_\perp$ (or p_y here). This did not happen in the simulations. Moreover, it is improbable that a Weibel-type instability will lead to the compression in density observed. We have also ruled out electrostatic interactions as a cause

of breakup since the electrostatic energy never accounts for more than 10^{-4} of the wave or kinetic energy because of the lack of charge separation between electrons and positrons. (If the ions were not positrons, electrostatic effects would indeed contribute to the breakup of the input waveform through various parametric instabilities.[13]) One possibility might be that the dielectric function of the plasma changes as the particles exchange energy with the waves through relativistic effects: Temporal modulation of the wave-particle interaction may then result. This mechanism should at least require a time of the bulk energy change to give rise to a major wave modification. As we have seen in the previous sections, however, a longitudinal density wave sets up in a time much shorter than the above. This is what leads to a breakup of both sinusoidal and sawtooth input waveforms through strong modulation of the perpendicular current density.

Irrespective of the initial waveform, the final quasistationary state seems to be a plasma very hot in the p_x direction, with twice as many peaks in the density as in the fields. The p_y momenta exhibit much less heating and preserve the original shape to a certain degree.

Irrespective of initial waveform and frequency, the relativistic wave accelerates the particles in the direction of propagation through the $\vec{v}\times\vec{B}$ force. The maximum momentum achieved p_x/m_0c is a few times the strength parameter ν in rough agreement with theory.[2,4] We recently simulated the interaction of an ultrarelativistic electromagnetic pulse in an underdense electron-positron plasma.[14] There the extent of the pulse was only about 1/100 of the plasma size, whereas here the wave extends over the whole plasma. For the pulse, the maximum momentum achieved through $\vec{v}\times\vec{B}$ acceleration scaled as $p_x/m_0c\sim\nu^2$. It would then appear that a continuous wave induces a maximum momentum about $1/\nu$ smaller than a pulse of the same peak amplitude.

Irrespective of initial waveform and frequency, the relativistic wave in an overdense electron-positron plasma generates or maintains a large longitudinal particle flux $\Gamma\lesssim 2n_0ec$. The longitudinal flux decreases as the wave frequency approaches relativistic cutoff. However, this decrease is steeper than the ratio of the phase velocities predicted from theory. The tendency towards equipartition of electromagnetic and particle fluxes is more pronounced as the wave shape steepens towards a sawtooth one; in the sawtooth start this equipartition is preserved even though the wave is destroyed. In addition, when the wave is initially and uniformly immersed in the plasma with frequency below the cutoff, the wave can still progress overall in time and accelerates particles forward.

In 1967, Pacini[15] suggested that angular momentum and rotational energy would be carried away from rotating magnetized neutron stars by an electromagnetic wave of immense amplitude. After the discovery of pulsars, it was found that the wave model accounted semiquantitatively for the observed lengthening of pulsar periods. Unfortunately, this model cannot be correct in its simplest form, because Goldreich and Julian[16] showed that surface field emission would fill the surrounding space with charged particles. Thus the electromagnetic wave propagates not in vacuum but in a plasma. Subsequently, Sturrock[3] showed that electron-positron pairs would be produced on current carrying field lines near the pulsar polar cap, and Ruderman and Sutherland[17] argued that those magnetized rotating neutron stars we observe as radio pulsars all have copious pair production. As the pulsar ages, it decelerates rotationally and eventually passes below the threshold for pair production, at which point it is radio silent. However, by far the majority of rotating magnetized neutron stars would be defunct pulsars, according to this reasoning.

The above developments motivated a line of basic research aimed at delineating the properties of nonlinear *plasma* waves of ultrarelativistic amplitude. Reasons of analytic tractability limited this research generally to plane waves in two-fluid theory. The results of this program have been summarized in Kennel *et al.*[18]; it appears that pulsars above pair-production threshold produce too dense a plasma for at least plane waves to propagate. However, defunct radio pulsars could radiate ultrarelativistic plasma waves. In addition, other astrophysical objects, such as radio galaxies or quasars, could conceivably radiate such waves into the tenuous plasma presumably filling intergalactic space. For these reasons, the continued development of the theory of ultrarelativistic plasma waves remains desirable. Our present results may be of interest to astrophysics in the following way. Regardless of the wave frequency or waveform, and whether or not the waveform is preserved, the original wave energy was rapidly converted into a mixture of ultrarelativistic particles and waves. Thus, wave energy should be effi-

ciently converted to cosmic rays. However, it seems likely that a single wave of immense amplitude will not exist long enough to be observable.

ACKNOWLEDGMENTS

The authors would like to thank J. Arons, C. E. Max, R. Pellat, and K. Quest for valuable discussions. This work was partially supported by National Science Foundation Contracts Nos. PHY-79-01319 and ATM-79-26492, National Aeronautics and Space Administration Grants Nos. NSG-7341 and NAGW-78, and by California Space Institute computing Grant No. CS79-9.

---

*Permanent address: Institute for Fusion Studies, University of Texas, Austin, Texas 78712.

[1]C. E. Max and F. W. Perkins, Phys. Rev. Lett. 27, 1342 (1971).
[2]C. F. Kennel, G. Schmidt, and T. Wilcox, Phys. Rev. Lett. 31, 1364 (1973).
[3]P. A. Sturrock, Astrophys. J. 164, 529 (1971).
[4]C. F. Kennel and R. Pellat, J. Plasma Phys. 15, 335 (1976).
[5]A. Decoster, Phys. Rep. 47, 285 (1978).
[6]P. K. Kaw and J. M. Dawson, Phys. Fluids 13, 472 (1979).
[7]A. B. Langdon and B. F. Lasinski, in *Methods in Computational Physics,* edited by B. Alder *et al.* (Academic, New York, 1976), Vol. 16, p. 300.
[8]A. T. Lin, J. M. Dawson, and H. Okuda, Phys. Fluids 17, 1995 (1974).
[9]T. Tajima and J. M. Dawson, Phys. Rev. Lett. 43, 267 (1979).
[10]J. M. Wersinger, J. M. Finn, and E. Ott, Phys. Fluids 23, 1142 (1980).
[11]E. Asseo, X. Llobet, and G. Schmidt, Phys. Rev. A 22, 1277 (1980).
[12]E. S. Weibel, Phys. Rev. Lett. 2, 83 (1959).
[13]C. E. Max, Phys. Fluids 16, 1480 (1973).
[14]M. Ashour-Abdalla, J. N. Leboeuf, T. Tajima, C. F. Kennel, and J. M. Dawson, Phys. Rev. A 23, 1906 (1981).
[15]F. Pacini, Nature 216, 567 (1967).
[16]P. Goldreich and W. H. Julian, Astrophys. J. 157, 869 (1969).
[17]M. A. Ruderman and P. G. Sutherland, Astrophys. J. 196, 51 (1975).
[18]C. Kennel, F. S. Fujimura, and R. Pellat, Space Sci. Rev. 24, 407 (1979).